# Overview of ASDEX Upgrade Results

H. Zohm, J. Adamek[1], C. Angioni, G. Antar[2], C.V. Atanasiu[3], M. Balden, W. Becker, K. Behler, K. Behringer, A. Bergmann, T. Bertoncelli, R. Bilato, V. Bobkov, J. Boom, A. Bottino, M. Brambilla, F. Braun, M. Brüdgam, A. Buhler, A. Chankin, I. Classen, G.D. Conway, D.P. Coster, P. de Marné, R. D′Inca, R. Drube, R. Dux, T. Eich, K. Engelhardt, H.-U. Fahrbach, L. Fattorini[4], J. Fink, R. Fischer, A. Flaws, M. Foley[5], C. Forest[6], J.C. Fuchs, K. Gál[7], M. García Muñoz, M. Gemisic Adamov, L. Giannone, T. Görler, S. Gori, S. da Graça, H. Greuner, O. Gruber, A. Gude, S. Günter, G. Haas, D. Hahn, J. Harhausen, T. Hauff, B. Heinemann, A. Herrmann, N. Hicks, J. Hobirk, M. Hölzl, D. Holtum, C. Hopf, L. Horton, M. Huart, V. Igochine, M. Janzer, F. Jenko, A. Kallenbach, S. Kálvin[7], O. Kardaun, M. Kaufmann, M. Kick, A. Kirk[8], H.-J. Klingshirn, G. Koscis[7], H. Kollotzek, C. Konz, K. Krieger, T. Kurki-Suonio[9], B. Kurzan, K. Lackner, P.T. Lang, B. Langer, P. Lauber, M. Laux, F. Leuterer, J. Likonen[10], L. Liu, A. Lohs, T. Lunt, A. Lyssoivan[11], C.F. Maggi, A. Manini, K. Mank, M.-E. Manso[4], M. Mantsinen[9], M. Maraschek, P. Martin[12], M. Mayer, P. McCarthy[5], K. McCormick, H. Meister, F. Meo[13], P. Merkel, R. Merkel, V. Mertens, F. Merz, H. Meyer[8], A. Mlynek, F. Monaco, H.-W. Müller, M. Münich, H. Murmann, G. Neu, R. Neu, J. Neuhauser, B. Nold[14], J.-M. Noterdaeme, G. Pautasso, G. Pereverzev, E. Poli, S. Potzel, M. Püschel, T. Pütterich, R. Pugno, G. Raupp, M. Reich, B. Reiter, T. Ribeiro[4], R. Riedl, V. Rohde, J. Roth, M. Rott, F. Ryter, W. Sandmann, J. Santos[4], K. Sassenberg[5], P. Sauter, A. Scarabosio, G. Schall, H.-B. Schilling, J. Schirmer, A. Schmid, K. Schmid, W. Schneider, G. Schramm, R. Schrittwieser[15], W. Schustereder, J. Schweinzer, S. Schweizer, B. Scott, U. Seidel, M. Sempf, F. Serra[4], M. Sertoli, M. Siccinio, A. Sigalov, A. Silva[4], A.C.C. Sips, E. Speth, A. Stäbler, R. Stadler, K.-H. Steuer, J. Stober, B. Streibl, E. Strumberger, W. Suttrop, G. Tardini, C. Tichmann, W. Treutterer, C. Tröster, L. Urso, E. Vainonen-Ahlgren[10], P. Varela[4], L. Vermare, F. Volpe, D. Wagner, C. Wigger, M. Wischmeier, E. Wolfrum, E. Würsching, D. Yadikin, Q. Yu, D. Zasche, T. Zehetbauer, M. Zilker.

Max-Planck-Institut für Plasmaphysik, EURATOM Association-IPP, 85748 Garching, Germany, [1] Institute of Plasma Physics, Praha, Czech, [2] University of Beirut, Lebanon, [3] Institute of Atomic Physics, EURATOM Association-MEdC, Romania, [4] CFN, EURATOM Association-IST Lisbon, Portugal, [5] Physics Dep., University College Cork, Association EURATOM-DCU, Ireland, [6] University of Wisconsin, Madison, USA, [7] KFKI, EURATOM Association-HAS, Budapest, Hungary, [8] UKAEA Culham, EURATOM Association-UKAEA, United Kingdom, [9] HUT, EURATOM Association-Tekes, Helsinki, Finland, [10] VTT, EURATOM Association-Tekes, Espoo, Finland, [11] LPP-ERM/KMS, EURATOM Association-Belgian State, Brussels, Belgium, [12] Consorzio RFX, EURATOM Association-ENEA, Padova, Italy, [13] Risø, EURATOM Association-RISØ, Roskilde, Denmark, [14] Institut für Plasmaforschung, Stuttgart University, Germany, [15] University of Innsbruck, EURATOM Association-ÖAW, Austria.

e-mail contact of main author: zohm@ipp.mpg.de

**Abstract**. ASDEX Upgrade was operated with fully W-covered wall in 2007 and 2008. Stationary H-modes at the ITER target values and improved H-modes with H up to 1.2 were run without any boronisation. The boundary conditions set by the full W-wall (high enough ELM frequency, high enough central heating and low enough power density arriving at the target plates) require significant scenario development, but will apply to ITER as well. D retention has been reduced and stationary operation with saturated wall conditions has been found. Concerning confinement, impurity ion transport across the pedestal is neoclassical, explaining the strong inward pinch of high-Z impurities in between ELMs. In improved H-mode, the width of the temperature pedestal increases with heating power, consistent with a $\beta_{pol,ped}^{1/2}$ scaling. In the area of MHD instabilities, disruption mitigation experiments using massive Ne injection reach volume averaged values of the total electron density close to those required for Runaway suppression in ITER. ECRH at the q=2 surface was successfully applied to delay density limit disruptions. The characterisation of fast particle losses due to MHD has shown the importance of different loss mechanisms for NTMs, TAEs and BAEs. Specific studies addressing the first ITER operational phase show that O1 ECRH at the HFS assists reliable low-voltage breakdown. During ramp-up, additional heating can be used to vary $l_i$ to fit within the ITER range. Confinement and power threshold in He

are more favourable than in H, suggesting that He operation could allow to assess H-mode operation in the non-nuclear phase of ITER operation.

## 1. Introduction

ASDEX Upgrade is a medium size divertor tokamak (R=1.65 m, a=0.5 m) with elongated cross-section, flexible shaping capability and versatile heating and current drive systems [1]. The goal of the ASDEX Upgrade programme is to give physics input to critical elements of the ITER design and the preparation of ITER operation. To this end, physics studies in the area of exhaust, transport, MHD stability and fast particle physics have been carried out and are reported in this overview. We also report on dedicated studies concerning the first operational phase of ITER, namely experiments on start-up scenarios and on confinement and L-H threshold in H and He.

The main hardware enhancement to ASDEX Upgrade, for the 2007 and 2008 campaigns, was the final step to a fully tungsten (W) coated wall (see Fig. 1), allowing to study the behaviour of W as a wall material in a divertor tokamak under ITER relevant conditions. This is of particular importance since it now becomes clear that C cannot be used in a fusion reactor due to its too high erosion rate and its unfavourable T retention. The latter property has recently led ITER to completely abandon C from its planning for the nuclear operation phase. Hence, a main focus of the ASDEX Upgrade programme in 2007 and 2008 was to investigate the compatibility of integrated ITER operational scenarios with the full W-wall.



*Fig. 1: A view into the fully W-covered ASDEX Upgrade vessel.*

## 2. Exhaust and Plasma Wall Interaction

In early 2007, the final step to a fully W-coated first wall was completed in ASDEX Upgrade [2]. All Plasma Facing Components (PFCs) are now C-tiles with W-coating, using a thick (200 μm) coating in the outer divertor and thin (~5 μm) coating in the other areas which usually see less power and particle flux during plasma operation. After a removal of boron layers and since no boronisation was applied in the first year of operation with the full-W wall (including the start-up), very clean experimental conditions to characterise the W-behaviour were met.

The W-sources due to plasma erosion were characterised in detail by spectroscopic methods, measuring the flux of W from the PFC into the plasma. This revealed that the highest influx originates from the outer divertor, with the ELM impact producing a large fraction of the W erosion, varying from 40 to 90 % depending on divertor conditions as the influx between ELMs decreases with decreasing electron temperature at the target [3]. In spite of producing the largest influx, the divertor erosion does not usually determine the W content of the discharge, hinting at a strong W-retention of the divertor. The clearest correlation between W influx and W content in the plasma is usually found for the outboard limiters, which appear to have a very high W fuelling efficiency. This especially poses a problem for the operation of ICRH in the all-W ASDEX Upgrade, where light impurities accelerated in the rectified sheath potential on field lines connecting to the W-coated ICRH limiters produce a large W influx that often leads to unacceptable W-concentrations in the plasma [4]. We note here that the W concentration is ultimately determined by the plasma transport, not only by the W-source (see

more details in Section 5). The total W erosion from PFCs is quite low (of the order 1 nm per discharge at most), so that in future, thin W-coatings will be used everywhere in the machine since the thick coatings experienced thermal problems, including cases of delamination after being exposed to high ELM averaged heat loads above 10 MW/m$^2$.

The transition to an all-W machine was also expected to greatly reduce the C-content of the plasma. Although the deposition of C in the inner divertor decreased by a factor of ~15 after installation of W-coated low field side limiters, indicating a drastic reduction of the source, the typical C-concentration in the plasma was only slightly reduced and is now of the order of 0.5-1 %, with the value transiently decreasing to 0.1-0.2 % after boronisation. This behaviour is attributed to the remaining C-sources (arcs cutting through the thin coatings and erosion from non-coated sides of the tiles) in combination with the recycling nature of C that makes it difficult to remove. On the other hand, after start-up with well-cleaned tiles and without boronisation, the B concentration did drop below the detection limit (estimated to be 0.1 %).

Regarding the gas balance of the machine, it was found that the change to full-W PFCs had a noticeable effect on the amount of He found in the plasma after He glow discharge cleaning. This technique had been applied in ASDEX Upgrade previously without detrimental effect, but led, in the full W-machine, to a quite high He-concentration of several 10 % which in turn led to deterioration of confinement. This change can be explained by the fact that W stores and releases He more easily than graphite [5]. After omission of the intershot glow discharge cleaning (except after disruptions, where D glow was applied), the He concentration was brought back to low levels and good H-mode confinement could be achieved readily (see also Section 5).

Concerning fuel retention, the detailed time resolved D gas balance was evaluated by carefully measuring the different influxes (valves and NBI fuelling) as well as the pumped gas by turbo molecular pumps and the cryo pump [5]. This allows to separate the initial phase where the wall pumps and the final outgassing during ramp-down from the phase where steady state plasma conditions prevail. Fig. 2 shows an example with a high gas puff. It can be seen that wall saturation does occur with the full W-wall in ASDEX Upgrade, with a retention that is zero within the error bars, the exact value being



Fig. 2: Gas balance for a high density AUG discharge with W-wall. Wall saturation is achieved in the late flat-top phase (3-4 s).

1.5 ± 3.2 %. This is notably different from earlier experiments with a C-wall which always showed finite retention, under the caveat that B from boronisation was always present in these discharges, whereas the behaviour quoted for the full W-wall refers to the unboronised, cleaned conditions in the beginning of the 2008 campaign. The overall shot integrated D-retention, which for the W-wall is then dominated by the difference between wall loading and outgassing in the start-up and ramp-down varies between 100% at very low density and 5% for semi-detached H-modes at high density, i.e. ITER relevant conditions. For ITER, where long pulses with high density are expected, one would expect the steady state phase to dominate the retention and hence a very small value for full-W conditions. These findings are
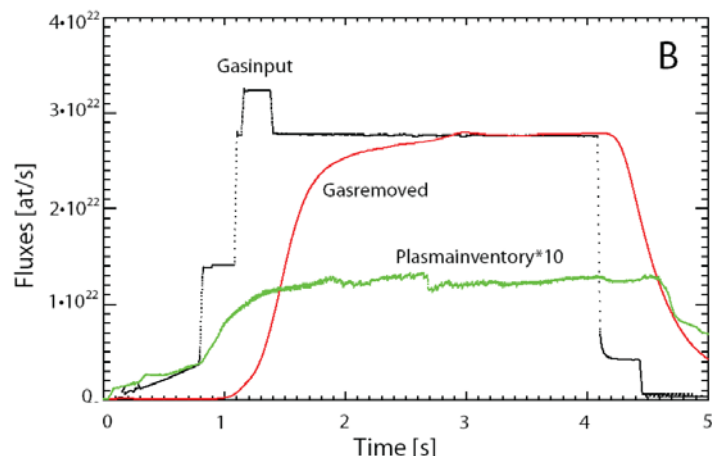
backed up by campaign integrated measurements of D retention in special marker tiles which show a pronounced reduction from 2.6% under C-dominated conditions to 0.6 % for the clean W-wall. While the main contribution to this number previously came from remote areas, indicating a role of D bound in a-CH films, now the outer divertor dominates due to direct implantation of D with the plasma flux. In summary, these results support the recent prediction of low T-retention values for ITER in case of a full-W wall [7].

## 3. Transport and fluctuation studies

While the first-principles understanding of core kinetic profiles has progressed significantly in the last years, this is not true for the pedestal profiles. Yet, they are decisive for determining fusion performance since the pedestal top sets the boundary conditions for stiff temperature profiles. On ASDEX Upgrade, we have therefore continuously upgraded the edge and pedestal diagnostics to achieve the required sub-cm and sub-ms resolution for all kinetic profiles. This included the recent commissioning of a new edge CXRS system for $v_{tor}$ and $T_i$ and the use of integrated data analysis, e.g. to infer density profiles form combination of Li-beam and DCN/$CO_2$ interferometry.

Previous studies had found $\eta_e = L_{ne}/L_{Te}$ in the range 1.5-2.2 in the edge transport barrier [8], with the lower values occurring at highest heating power and low gas fuelling. For the ions, using the new diagnostics capabilities, we evaluate $\eta_i \approx 1$. Once the H-mode is developed, transport analysis indicates that impurity density and ion temperature profiles can be described using neoclassical transport [9]. This also holds for the time evolution during the ELM cycle; in particular, the strong inward drift of high-Z impurities in between ELMs can be explained by the neoclassical inward pinch in the steep gradient region. This highlights the role of ELMs, which flush this zone from impurities, in regulating the penetration of W into the core plasma (see also section 5). A peculiar feature was found with the high resolution $v_{tor}$ measurements: in well-developed H-mode conditions, they show a minimum at the density pedestal top, with an actual increase of $v_{tor}$ along the radius towards the separatrix [10]. Interpretation of this finding is at present ongoing.

For given slope, the extent of the steep gradient region, the pedestal width, will set the pedestal top value. In improved H-mode, this width is found to increase with heating power, contributing to the improvement of the H-mode enhancement factor compared to the ITER98(y,2) scaling. Consistent with DIII-D and JT-60U, this trend can be described by a scaling $\Delta_p \sim \beta_{pol,ped}^{1/2}$ (see Fig. 3) [11]. Interestingly, this scaling comes from an increase in pedestal width of $T_e$, while the density pedestal width seems unchanged. For the cases with good diagnostic coverage, also the $T_i$ pedestal width is found to increase with heating power.



Fig. 3: the $T_e$ pedestal width scales with $\beta_{pol,ped}^{1/2}$ in improved H-mode at low $\delta$.

Concerning global confinement scalings, experiments on the β-dependence of transport showed a decrease of global H-mode confinement with $\beta^{-0.9}$ [12], consistent with the ITER98(y,2) scaling and in contradiction to a less pronounced scaling $\beta^{0.1}$ found in a previous series of DIII-D discharges [13]. Further work is required to sort out similarities and
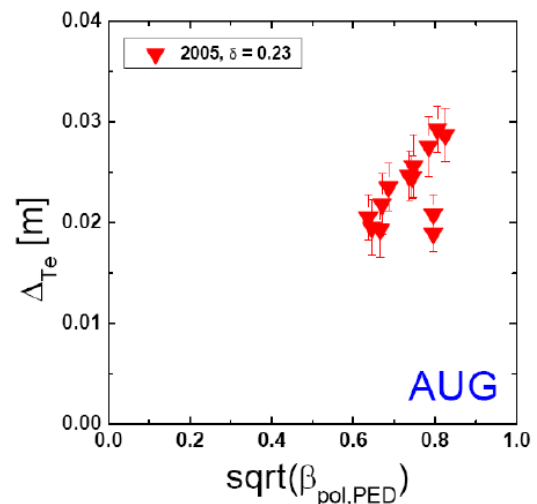
differences between these findings, since collisionality and rotation were not the same in the two experiments.

Fluctuation studies using Doppler reflectometry were continued [14]. The k-selectivity of this method allows to obtain k-spectra in a single discharge using a newly designed movable antenna pair. While L-mode spectra show a decrease of the fluctuation power with exponent 3-4, close to results from other devices and not far from an 'inertial regime' 8/3 (Kolmogorov), H-mode spectra taken well inside the pedestal ($\rho_p = 0.78$) show a surprisingly large exponent of 7 or more, indicating that at least one of the conditions for the inertial range is violated, such as the self-similarity of the cascade process. The flatter H-mode density profile could of course also lead to a reduced drive so that the dissipative range is already encountered at these values of $k\rho \gg 1$, which are much larger than the range expected for the turbulence responsible for anomalous transport from linear calculations ($k\rho \leq 1$).

Doppler reflectometry is also used to characterise Geodesic Acoustic Modes (GAMs), which so far have only been observed in OH and L-Mode discharges [14]. Inside the pedestal top radius, the GAM dispersion relation is found to fit well with simple theory predictions for circular plasmas, but outside is has an additional shape and q dependence. The GAM frequency does not change continuously with radius, but rather exhibits radial plateaus of constant frequency, reminiscent of zonal flow behaviour. The GAM amplitude increases with $\nabla T_e$, i.e. turbulent drive and seems to be determined by the balance between that drive and Landau damping.
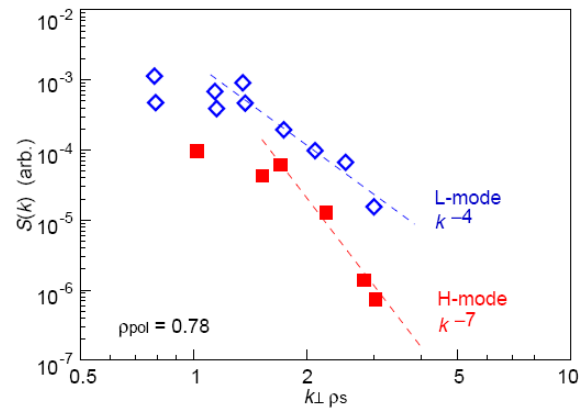


*Fig. 4: Density fluctuation spectra obtained by Doppler reflectometry in L- and H-mode.*

Concerning turbulence in the SOL, we have used a 'filament probe' (array of Langmuir probes and pick-up coils) to characterise the radial and poloidal motion of filaments expelled into the SOL [15]. We find a tendency for the radial velocity to increase with filament density and size, supporting models balancing the charge separation by diamagnetic currents [16]. Comparable radial decay lengths of particle and heat flux as measured by Langmuir probes and thermography demonstrate that the energy loss from the filament in the far SOL is dominated by ion convection with ion energies of $T_i \approx 30 \div 60 eV$ and $T_i > T_e$.

## 4. MHD Instabilities

Concerning ELMs, the ASDEX Upgrade programme continues to investigate ELM pacing by pellets. Recent studies have addressed the physics of ELM triggering by pellets [17]. We find that all pellet speeds and sizes used so far on ASDEX Upgrade seem to introduce a similar local pressure perturbation on their ablation path. This would mean that even the smallest pellets used so far lead to a saturation of the local perturbation, e.g. by tapping all available energy on a flux surface. We find that this perturbation can reliably trigger a type I ELM at almost any phase of the ELM cycle, indicating a metastability of the ELM during most of its cycle such that it can be triggered by a finite amplitude perturbation. Hence, even much smaller pellets should be able to reliably trigger ELMs. This will be tested in the near future when the existing blower gun has been modified to produce smaller pellets.

ASDEX Upgrade regularly uses a fast gas valve injecting Ne into the plasma when a disruption is approached (as determined from a locked mode detector) to mitigate forces occurring during the concomitant vertical displacement. These studies have been extended to investigate the possibility of achieving very high density in the disruption phase [18]. This will be crucial for ITER to prevent excessive runaway production (in ASDEX Upgrade, runaways are usually not produced during disruptions). Injecting Ne with an optimised valve close to the plasma can initiate the current quench only 2 ms after the trigger and shows fuelling efficiency $N_e/N_{atom}$ between 20 and 40 %, (30-60% for He), with no signs of degradation up to the highest amount of gas injected so far (several $10^{22}$ atoms). Line averaged density of up to $2 \times 10^{21}$ $m^{-3}$ has been reached, more than an order of magnitude higher than the plasma density before injection. Modelling with the SOLPS code package indicates that Ne is only singly ionised, such that the total (free plus bound) electron density is roughly an order of magnitude higher. Since for runaway generation, the total electron density must be considered, volume averaged values of $n_{e,tot}$ close to the the 'Rosenbluth' density of $n_{e,tot} = 4 \times 10^{22}$ $m^{-3}$ have been reached with this valve geometry.
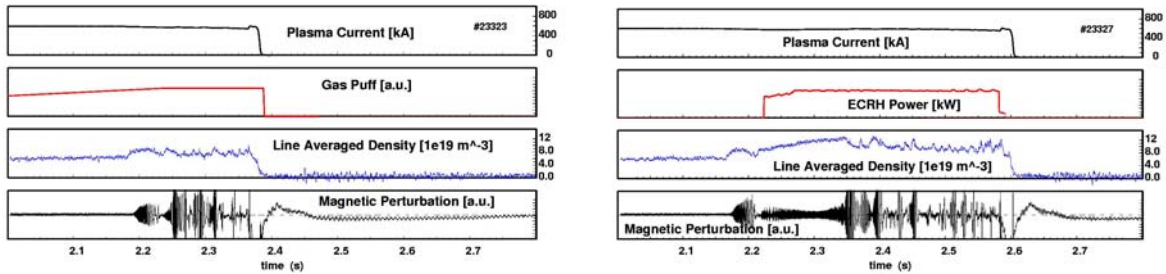


*Fig. 5: Delay of a density limit disruption by injecting 0.6 MW ECRH at the q=2 surface (right panel). A transient phase with low MHD activity occurs in which the density can be substantially increased.*

A scheme for active disruption avoidance was tested using ECRH in high $q_{95}$ density limit disruptions [19]. At this $q_{95}$ value, the disruption sequence begins with the occurrence of a MARFE on closed flux surfaces, destabilising a (3,1) tearing mode, followed by a (2,1) that locks and leads to the disruption. Similar to previous findings in FTU, the onset of the (2,1) mode could be delayed by injecting ECRH at the $q$=2 surface. If the ECRH is well aligned with $q$=2, a phase in which the density can be raised above the Greenwald limit is obtained. In this phase, the (2,1) mode attains a saturated low level before it ultimately grows rapidly and leads to disruptive termination. This is shown in Fig. 5. Further experiments will have to show if stable operation is possible at a higher density using this scheme (the gas puff was programmed to a high feed forward value in this series of experiments). Another purpose could be to use the delay time of the explosive (2,1) growth for corrective measures such as closing the gas puff or increasing the total heating power to recover the discharge.

A recent development at ASDEX Upgrade is the investigation of a possible role of stochastisation in fast MHD phenomena by using a fast mapping procedure to obtain Poincare plots in situations where multiple modes are present [20]. It is found that the experimentally determined level of (2,2) and (3,3) harmonics of the (1,1) mode observed before a sawtooth crash can induce significant stochstisation if the q profile inside $q$=1 drops low enough to offer sufficient resonant surfaces for interaction. This also offers an explanation for the observation that often, sawtooth crashes in ASDEX Upgrade show incomplete reconnection with a (1,1) postcursor remaining. Similarly, using the experimentally observed amplitudes of ideal (4,3) and neoclassical tearing (3,2) modes during a FIR-NTM crash, stochastisation is likely to play a role in the fast redistribution of temperature and the reconnection reducing the (3,2) NTM amplitude.

The studies of the interaction between fast ions and MHD modes using a fast ion loss probe (scintillator in a magnetic spectrometer) with high (~ 1 MHz) temporal resolution revealed a variety of new results [21]. From the temporal behaviour during NBI modulation, it was found that fast NBI particle losses due to NTMs occur on two timescales, namely the transit time of fast ions on drift islands intersecting the wall (~ 10 µs) and a component due to stochastic diffusion in the presence of overlapping drift islands (~ several ms). ICRH generated fast ions can be ejected due to a resonance between the rotating mode and the trapped particle orbit $n\omega_{prec}$-$p\omega_{bounce}$-$\omega_{<mode}=0$ (with $\omega_{mode} << \omega_{bounce}, \omega_{prec}$ for NTMs) [22].

Fast particle driven modes and their interaction with the fast ion population have been studied as well. Fig. 6 shows an example of a TAE induced particle loss where the resonant character of the loss can be clearly seen by the frequency match between losses and modes. In this figure, also a non-Alfvenic (i.e. the frequency variation does not correspond to a density variation) fast particle driven mode is seen in trace c). The dispersion relation of this mode is reasonably well described by the BAE formula which involves the sound speed due to the compressional character of the mode [23]. Due to its central location, this mode with mode numbers (4,4) is hardly seen on the magnetics diagnostic, but it enhances the fast particle losses by redistributing fast particles from the centre to half radius where they are then lost through the TAEs.
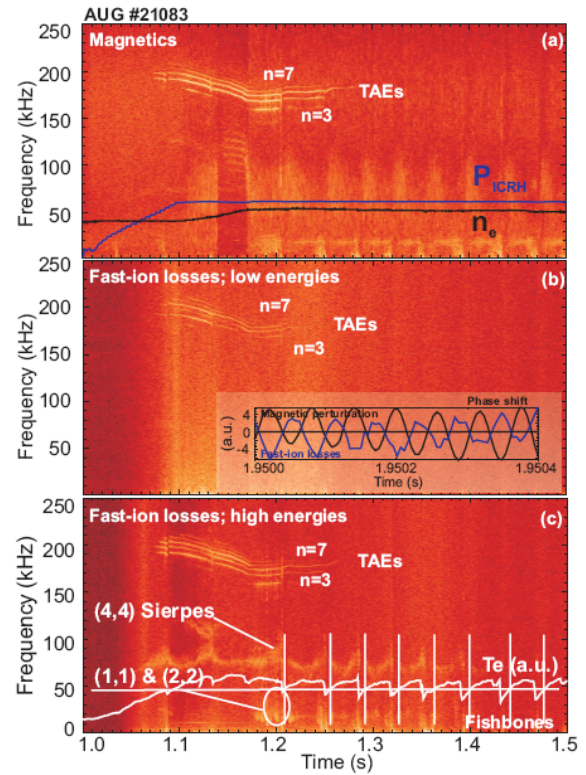


*Fig. 6: Fast particle losses due to modes driven by energetic particles: magnetic perturbation spectra a) and fast ion loss detector spectra c) show the same frequencies. The phase relation between them is shown in b) for a TAE.*

## 5. Scenario development with a full W-wall

A main aim of the W programme in ASDEX Upgrade is to study the compatibility of ITER operation scenarios with the full W-wall. Hence, the machine was operated for most of the 2 years without boronisation to investigate plasma operation with essentially uncovered W-surfaces. After adaptation of the glow discharge conditioning procedure as described in Section 2, stationary H-mode discharges at the ITER target ($H=1, \beta_N = 2$) in the density range $0.6 \leq n/n_{GW} \leq 0.8$ were readily achieved [24]. The upper limit in this density range comes from the low triangularity values that were used, due to the restrictions in power imposed by the temporary loss of one of three flywheel generators in 2006 (this generator will be back in operation in 2009). The lower limit comes from the operational necessity to always apply a finite gas puff level during the whole discharge in the full-W ASDEX Upgrade. This is mainly needed to ensure a high enough ELM frequency of at least ~ 50 Hz to prevent a too high influx of W in between ELMs. Since on the other hand, higher gas puff and ELM frequency tend to deteriorate confinement, the level of gas puff applied is an optimisation parameter in the present conditions.

An example is shown in Fig. 7, where the gas puff level has been varied, showing that the lowest ELM frequency has the highest confinement, but also the (in this case) still tolerable highest W concentration. Since also total heating power raises the ELM frequency, the level of gas puff can actually be decreased at higher NBI power, proving that transport across the ELM affected area and not the source from the PFCs is crucial for impurity accumulation.
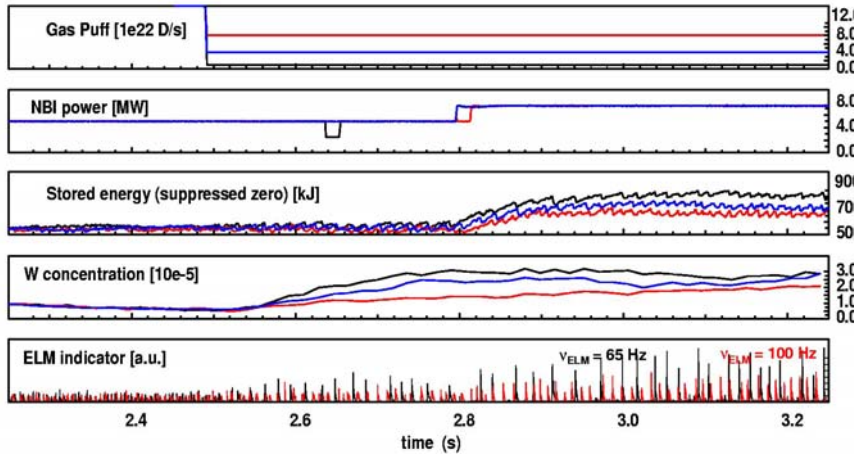


*Fig. 7: Optimisation of confinement by adjusting the gas puff level. Lower puff rate decreases the ELM frequency and increases the stored energy, but also the W-concentration.*

Another operational requirement imposed by the W-wall is that in most discharges, central heating to avoid central accumulation of W is needed. As reported before [25], ECRH has proven to be very effective in providing this central heating. We found that central deposition within $\rho < 0.2$ is essential to completely suppress accumulation. This behaviour has been modelled by taking into account the neoclassical inward pinch for W and the anomalous outward diffusion that is increased by the ECRH. Scaling this modelling to the $Q=10$ scenario in ITER, central $\alpha$-heating should be sufficient to prevent accumulation of W [26].

A third constraint comes from the power handling capability of the W-coated divertor tiles which do not allow exposure to average heat fluxes above 10 $MW/m^2$. After boronisation of the machine in 2008, the intrinsic impurity level (especially O) was reduced to such a low value that divertor radiation was not sufficient to limit the heat flux below this value even at 7.5 MW of NBI power with low density, a situation that had not been encountered in the C-machine. This led to tile damage and we will have to implement radiative cooling and pellet pacing to extend the operational space; a regime mandatory for any C-free reactor operation. On the other hand, after boronisation, the higher power across the separatrix meaning a higher ELM frequency, and the lower W-influx from the main chamber walls allowed to run stable discharges with zero gas puff; this was not possible without boronisation so far. Also, ICRH could be applied much more successfully with the



*Fig. 8: Dataset of improved H-mode discharges ($I_p = 1$ MA, PNBI=10-14 MW, $\delta < 0.32$) before (2003-20060 and after (2008) the transition to full W wall.*

reduced O-concentration after boronisation, even under conditions when the initial boron layer covering the ICRH antenna limiters was already removed by high power operation [4]. This is consistent with the assessment that low-Z impurities accelerated in the rectified sheath potential dominate the sputtering of W from the antenna limiters.
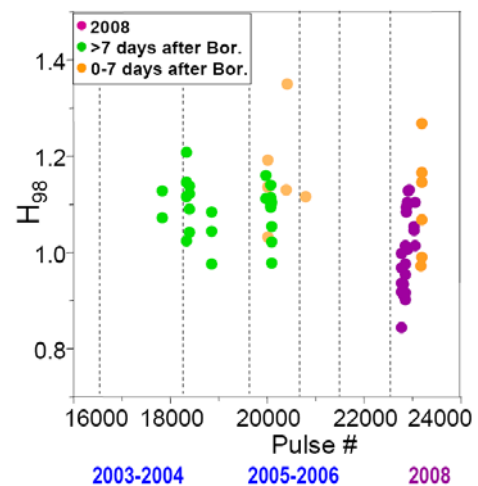
Concerning Advanced Operation, improved H-mode conditions could be accessed in stable operation even without boronisation, with the H-factor clearly exceeding 1 at lower gas puff. After boronisation and with zero gas puff, the confinement was back to the highest values obtained in the C-device at that triangularity. Fig. 8 shows this for a set of improved H-mode discharges collected from the experimental campaigns in the years 2003-2008. We note here that using ctr-ECCD in low density discharges without NBI, ITBs in the electron temperature, with central value $T_e \sim 20$ keV, were readily achieved as in previous campaigns.

## 6. Specific studies adressing the first ITER operational phase

In 2008, a series of experiments was carried out after the ITER central team had pointed out some specific open questions concerning the first ITER operational phase, namely the start-up with low loop voltage and control of $l_i$ as well as confinement and L-H mode threshold in H and He, the working gases foreseen for the non-nuclear ITER operation phase. These questions were addressed in an international effort, coordinated by the ITPA topical groups. This section summarises the experimental results in these areas obtained from ASDEX Upgrade; an overview of the joint experimental effort is given in [27].

Concerning start-up, ASDEX Upgrade was operated without additional resistors in the OH circuit, resulting in loop voltage values as low as 0.25 V/m (0.8 V/m with additional resistor, ITER foresees 0.33 V/m for start-up). Even at this lowest value of loop voltage, reliable breakdown and current ramp up was demonstrated using ECRH preionisation both with X2 and O1 mode. The O1 scenario was performed at 3.1 T and 105 GHz, putting the resonance on the HFS, equivalent to the use of the main heating gyrotron at 170 GHz and full field in ITER and showed very reliable start-up. Basically, the preionised plasma



Fig. 9: Variation of the $l_i$ value in flattop by using different heating schemes during ramp-up. The ITER target range is indicated in blue.

could be ramped up in current linearly with the transformer, with the ramp rate just depending on the loop voltage. This also allowed some variation in $l_i$. More control over $l_i$ was achieved using additional heating in the ramp-up phase, with L-modes achieving lower $l_i$ values than pure ohmic at the end of the flat-top and H-mode transition in the ramp-up phase leading to a further reduction in $l_i$. Fig. 9 shows different conditions obtained at constant current ramp rate but different heating powers, indicating that a variation over the ITER target range (0.7-1.0) is possible in this scenario.
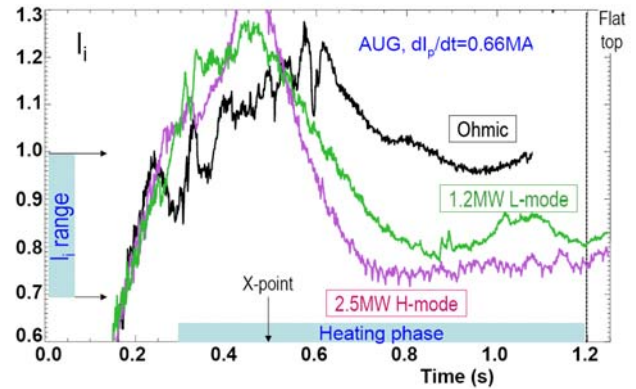
For its first operation phase, ITER cannot use D as working gas since the neutrons generated would make manned access difficult or impossible after relatively short operation time. Operation in H, on the other hand, may not allow to access the H-mode because the power threshold $P_{thr}$ is higher by about a factor of 2 than in D. Hence, there has been increasing interest in confinement and threshold of He plasmas [28]. A dedicated series of experiments in ASDEX Upgrade was done to address this subject, using NBI (injecting D or H) and ECRH (to access low densities). Confinement follows the global $I_p$ and $P$ scaling predicted by ITER98(p,y), but the absolute value is reduced by a factor of 0.7 with respect to the values obtained in D. This is still about 20% higher than for pure H operation. The reduction is partly caused by the lower ion density, but also by a degradation of the pedestal. Interestingly,

$P_{thr}$ is very similar to the values obtained for D, and hence a factor of ~ 2 lower than in H. This is shown for a density scan at constant magnetic field in Fig. 10, where one can also see that no difference exists between the values obtained with D-NBI, H-NBI and ECRH. We note that the minimum in $P_{thr}$ that has been found before in H and D also occurs in He at roughly the same value. These findings suggest that He would be a well suited working gas for the initial ITER operational phase to access the H-mode, which is required for integrated commissioning.



Fig. 10: comparison of the power threshold for the L-H transition in He (red) and D (black) using different heating schemes.

## 7. Hardware Extensions

A number of hardware enhancements to ASDEX Upgrade are under way to address open questions concerning the detailed ITER design or its operation. The ECRH enhancement to 6(4) MW at 2(10) s is progressing, but the envisaged multi-frequency gyrotrons are still awaiting the final solution for the window problem. Meanwhile, 2-frequency gyrotrons (105/140 GHz) using a single resonant window have been operated on ASDEX Upgrade successfully [29]. The fast steerable launcher has been commissioned and experiments concerning feedback control of the deposition will be started in 2009.

The installation of 24 in-vessel coils (3 sets of 8 coils in toroidal direction, see Fig. 11) is under way, with the first set of 8 coils to be installed in 2009 [30]. This design is very similar to the one presently foreseen for installation on ITER (3 x 9 coils in roughly the same poloidal location). The coils will allow experiments on ELM suppression using up to n=4 static fields, assessing how localised in radius the perturbation can be (present experiments do not exceed n=3). After installation of power supplies powering individual sets of coils, studies of the interaction of rotating helical fields with MHD modes will be possible. In a later stage, it is planned to install in addition a conducting shell in



Fig. 11: view of the 24 in-vessel coils to be installed from 2009 on.

ASDEX Upgrade to allow the use of the in-vessel coils for RWM stabilisation experiments.

As described above, ICRH operation is at present not fully compatible with high power operation in the presence of the fully W-covered first wall due to the prohibitive influx of W from the limiters. Analysis shows that the rectified sheath potential that accelerates impurities to create this influx could be reduced by using a 4-strap antenna, flush mounted in the wall [4]. This should greatly reduce the shielding currents in the antenna casing ('box currents') that have been identified as a main contributor to the sheath potential. Such an antenna concept can be stepwise tested in ASDEX Upgrade to solve the problem of compatibility of ICRH with high-$Z$ wall.

Further experimental work on scenario development will clearly need feedback control of the current profile. While such a control is being implemented in real-time at present on ASDEX Upgrade, the existing actuators are limited and hence a conceptual study for an LHCD system
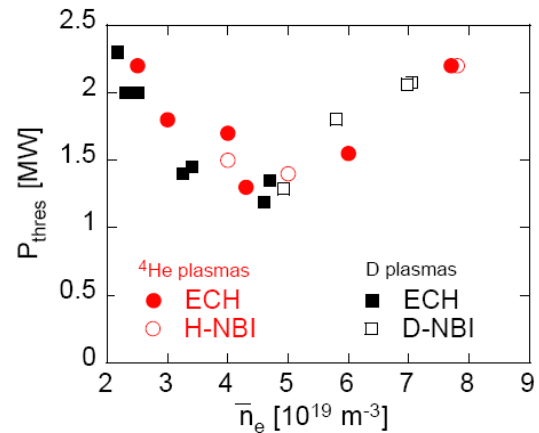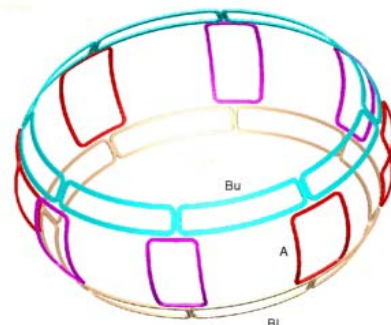
on ASDEX Upgrade has been undertaken by CEA Cadarache. It is found that a system launching 4 MW of 3.7 GHz waves through a PAM grill with $n_{||}$ = 2.5 could drive around half of the total plasma current in improved H-mode or ITB scenarios, allowing completely non-inductive operation to be assessed. Such a system could be installed in the future to greatly enhance the capabilities of ASDEX Upgrade in the area of steady-state tokamak research.

## 8. Summary and Conclusions

The operation of ASDEX Upgrade with the fully W-covered wall in 2007 and 2008 has shown that it is possible to access both stationary H-modes at the ITER target values and improved H-modes with H up to 1.2 without boronisation. Operational recipes had to be adjusted with the full W-wall to take into account the new boundary conditions. These are 1) a high enough ELM frequency to prevent too strong W-influx across the ELM affected zone, achieved by gas puff or high heating power; 2) a high enough central heating to prevent accumulation of W in the centre of the discharge, achieved by ECRH and 3) a low enough power density < 10 MW/m$^2$ arriving at the target plates. In the absence of divertor radiation by C and O, such as after a boronisation, condition 3) requires use of impurity seeding and pellet pacing to make use of the full heating power installed at ASDEX Upgrade. We note that all three boundary conditions will apply to ITER as well. Without boronisation, ICRH operation leads to a high influx of W from the antenna limiters due to sputtering by light impurities accelerated in the rectified sheath potential developing in front of the antenna. D retention has been reduced with the transition to full W-wall and with high gas puff, stationary operation with saturated wall is found. Due to this initial success, the future ASDEX Upgrade programme will keep the full W-coverage and continue to investigate the compatibility with ITER scenarios, also in view of the installation of a full-metal wall in JET in 2009/2010.

Concerning confinement, a characterisation of the pedestal with high temporal and spatial resolution using newly commissioned diagnostics shows that impurity ion transport across the pedestal is neoclassical, explaining the strong inward pinch of high-Z impurities in between ELMs. In improved H-mode, the width of the temperature pedestal increases with heating power, consistent with a $\beta_{pol,ped}^{1/2}$ scaling found for $\Delta_{Te}$. Density fluctuation spectra in H-mode show a surprisingly steep decay at high $k\rho >> 1$, with exponents of order 7 and above.

Disruption mitigation experiments using massive Ne injection using an optimised valve geometry have reached volume averaged values of the total (free plus bound) electron density close to those required for Runaway suppression in ITER. ECRH at the $q$=2 surface was successfully applied to delay density limit disruptions. The characterisation of fast particle losses due to MHD has shown the importance of different loss mechanisms for NTMs, TAEs and BAEs.

Specific studies addressing the first ITER operational phase show that O1 ECRH at the HFS using the gyrotrons for main heating assists reliable low-voltage breakdown. During the ramp-up, additional heating can be used to vary the $l_i$ value to fit within the ITER range at the beginning of the flattop. Confinement and power threshold in He are more favourable than in H, suggesting that He operation could allow to assess H-mode operation in the non-nuclear phase of ITER operation.

The ASDEX Upgrade programme will continue to address open questions concerning ITER design and operation. To that end several hardware enhancements are under way (ECRH upgrade, internal coils and conducting shell) or under consideration (LHCD with PAM

launcher). Also, the design of an ICRH antenna developing reduced sheath potential in front of the limiters will be investigated.

## References

[1]  ASDEX UPGRADE TEAM, Fusion Science and Technology **44** (2003) 1.

[2]  NEU R., et al., Plasma Phys. Control. Fusion **49** (2007) B59.

[3]  KALLENBACH A., et al., IAEA-CN-165/EX/9-2 (2008).

[4]  BOBKOV V., et al., IAEA-CN-165/EX/P6-31 (2008).

[5]  SCHMID K., et al., Nucl. Fusion **49** (2007) 984.

[6]  ROHDE V., et al., IAEA-CN-165/EX/P4-3 (2008).

[7]  ROTH J., Plasma Phys. Contr. Fusion **50** (2008) 103001.

[8]  NEUHAUSER J., et al., Plasma Phys. Control. Fusion **44** (2002) 855.

[9]  WOLFRUM E., IAEA-CN-165/EX/P3-7 (2008).

[10] PÜTTERICH T., et al., submitted to Phys. Rev. Lett (2008)

[11] MAGGI C.F., et al., Nucl. Fusion **47** (2007) 535.

[12] VERMARE L., et al., Nucl. Fusion **47** (2007) 490.

[13] PETTY C.C., et al., Phys. Plasmas **11** (2004) 5.

[14] CONWAY, G.C., IAEA-CN-165/EX/P5-38 (2008).

[15] SCHMID, A., et al. , Plasma Phys. Control. Fusion **50** (2008) 4.

[16] GARCIA O. E., et al., Physics of Plasmas **13** (2006).

[17] LANG P. IAEA-CN-165/EX/P4-5 (2008).

[18] PAUTASSO G. IAEA-CN-165/EX/P9-1 (2008).

[19] ESPOSITO B. IAEA-CN-165/EX/P7-3 (2008).

[20] IGOCHINE V. IAEA-CN-165/EX/P9-10 (2008).

[21] GARCIA-MUNOZ M. IAEA-CN-165/EX/6-1 (2008).

[22] POLI E., et al., Physics of Plasmas **15** (2008) 032501.

[23] LAUBER P., et al., 35th EPS Conference on Plasma Physics, Hersonissos, Crete, (2008).

[24] GRUBER O. IAEA-CN-165/EX/P1-5 (2008).

[25] NEU R., et al., Plasma Phys. Control. Fusion **44** (2002) 811.

[26] DUX R., et al., IAEA-CN-116/EX/P6-14 (2004).

[27] SIPS A.C.C., et al., IAEA-CN-165/IT/2-2 (2008).

[28] RYTER F., et al., IAEA-CN-165/EX submitted as post-deadline paper (2008).

[29] WAGNER D., et al., Nucl. Fusion **48** (2008) 054006.

[30] SUTTROP W., et al., submitted to Fus. Eng. Des. (2008).